nature astronomy

Article

https://doi.org/10.1038/s41550-024-02342-4

The formation of the TRAPPIST-1 system in two steps during the recession of the disk inner edge

Received: 1 June 2023

Accepted: 16 July 2024

Published online: 20 August 2024

Check for updates

Gabriele Pichierri[1,2] ✉, Alessandro Morbidelli[3,4], Konstantin Batygin[1] & Ramon Brasser[5,6]

TRAPPIST-1 hosts seven planets. The period ratios of neighbouring pairs are close to the 8:5, 5:3, 3:2, 3:2, 4:3 and 3:2 ratios in increasing distance from the star. The Laplace angles associated with neighbouring triplets are observed to be librating, proving the resonant nature of the system. This compact, resonant configuration is a manifest sign of disk-driven migration; however, the preferred outcome of such evolution is the establishment of first-order resonances, not the high-order resonances observed in the inner system. Here, we explain the observed orbital configuration with a model that is largely independent of the specific disk migration and orbital circularization efficiencies. Together with migration, the two key elements of our model are that the inner border of the protoplanetary disk receded with time and that the system was initially separated into two subsystems. Specifically, the inner b, c, d and e planets were initially placed in a 3:2 resonance chain and then evolved to the 8:5–5:3 commensurability between planets b, c and d due to the recession of the inner edge of the disk, whereas the outer planets migrated to the inner edge at a later time and established the remaining resonances. Our results pivot on the dynamical role of the presently unobservable recession of the inner edge of protoplanetary disks. They also reveal the role of recurring phases of convergent migration followed by resonant repulsion with associated orbital circularization when resonant chains interact with migration barriers.

The main difficulty in explaining the observed[1,2] orbital configuration of the TRAPPIST-1 system consists in reproducing the inner planets' 8:5 and 5:3 period ratios combined with the outer planets' vicinity to first-order 3:2 and 4:3 resonances. *N*-body simulations of the full seven-planet TRAPPIST-1 system undergoing classical[3,4] disk-driven type-I migration show that the natural outcome of this scenario is the formation of a simpler first-order 3:2–3:2–3:2–3:2–4:3–3:2 resonant chain[5,6]. Reference 7 argued for a two-subsystem structure based on the libration of Laplace angles but noted that the observed period ratios could be obtained from the disk-driven migration by adjusting the migration and eccentricity-damping timescales. Reference 8 showed that the 8:5 and 5:3 ratios can be built from an original 3:2–3:2 resonance if planets enter the inner cavity of the disk. Their model contains two critical assumptions. First, it invokes enhanced disk-driven eccentricity damping (about 50 times more efficient than expected for typical type-I migration), which was found to be advantageous for obtaining the observed TRAPPIST-1 resonant chain. Second, it involves a requirement on the timing of arrival of the outer planets to ensure that

[1]Division of Geological and Planetary Sciences, California Institute of Technology, Pasadena, CA, USA. [2]Max Planck Institute for Astronomy, Heidelberg, Germany. [3]Laboratoire Lagrange, Université Cote d'Azur, CNRS, Observatoire de la Cote d'Azur, Nice, France. [4]Collège de France, CNRS, PSL Univ., Sorbonne Univ., Paris, France. [5]Konkoly Observatory, HUN-REN Research Centre for Astronomy and Earth Sciences, MTA Centre of Excellence, Budapest, Hungary. [6]Centre for Planetary Habitability, University of Oslo, Oslo, Norway. ✉e-mail: gabe@caltech.edu

https://doi.org/10.1038/s41550-024-02342-4

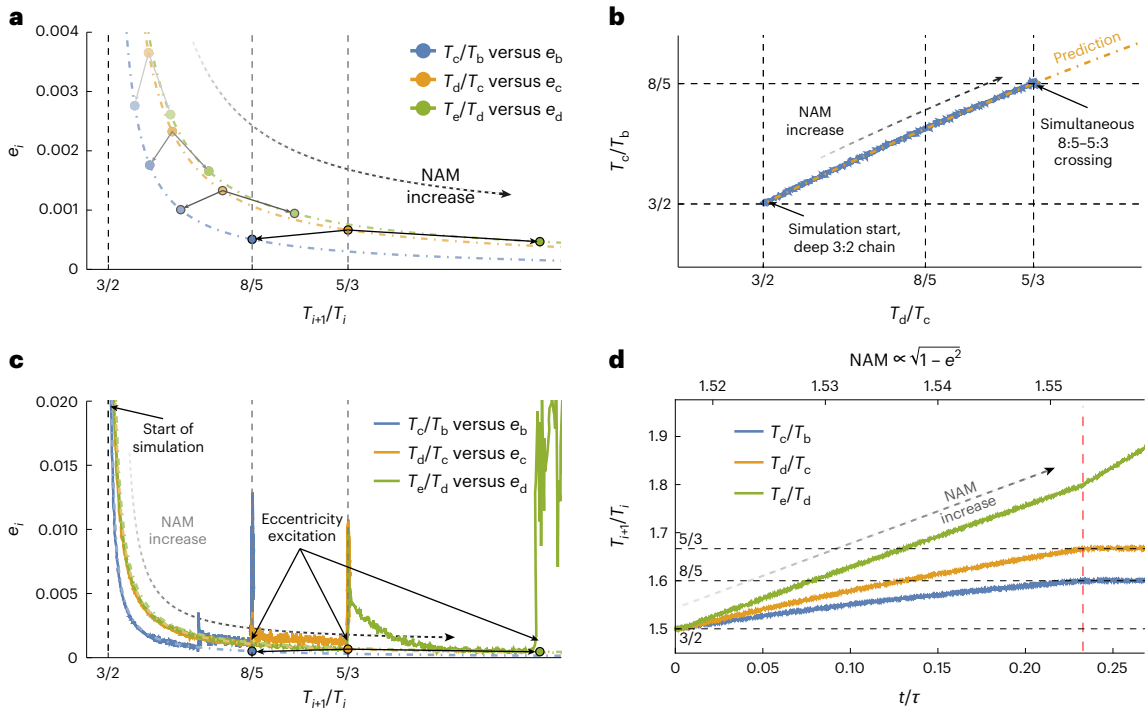

Fig. 1 | Evolution of a 3:2 resonant chain under dissipation. a, Coloured dotted-dashed curves show predicted equilibria for a TRAPPIST-1b, c, d and e system locked in a 3:2–3:2–3:2 resonance in the orbital period ratio versus eccentricity (e) plane for various NAM values (the global resonant gauge of the system's state, which increases as indicated by the dashed arrow). When the planets are deep in resonance, their orbital state must be in an equilibrium state determined solely by the NAM. Four fixed values of the NAM were chosen for explanatory purposes. The corresponding equilibrium period ratios and eccentricities of the four planets are all linked, as shown by the arrows. For one of them (arrows in black), $T_c/T_b \simeq 8/5$ and $T_d/T_c \simeq 5/3$, which are the presently observed period ratios of these planets. **b**, Simultaneous crossing of the 8:5–5:3 resonance in the b–c versus c–d period ratios plane in a simulation of the TRAPPIST-1b, c, d and e system starting from a deep 3:2 chain as the NAM increases in time. **c**, Evolution in the period ratio versus e plane (as in **a**). Lighter coloured dotted-dashed lines are the same as in **a**, whereas continuous lines represent the simulated evolution (some lines are on top of each other). Notice the kick in the eccentricity at the simultaneous crossing of the 8:5–5:3 resonance for planets b–c–d. **d**, For the same run, coloured continuous lines show the evolution of the period ratios over time (expressed in units of a timescale τ in the bottom axis) as the NAM increases (top axis). The simultaneous 8:5–5:3 crossing (predicted in the top panels) is indicated by a vertical dashed red line.

the inner system does not evolve past the 8:5–5:3 ratios. Planet e must enter into resonance with planet d at the appropriate time to block the migration of planet c into a three-body c–d–e Laplace resonance when the former is in the right orbital position. The existence and extent of the appropriate time window depend on the migration parameters introduced to mimic planet–disk interactions. Drawing from these ideas, we develop a model whose key elements are independent of the disk migration parameters, which thereby removes the need for specific disk migration and damping efficiencies. Our model invokes a simple timing constraint for the arrival of the outer planets that depends only on the rate of recession of the inner edge of the disk.

As in refs. 7,8, we considered inner and outer TRAPPIST-1 subsystems. The first step was to consider the evolution of the inner system alone near the favoured 3:2 commensurabilities. Specifically, we investigated how the orbital period ratios could increase so that the 8:5–5:3 period ratios for planets b, c and d are reached and how this resonant repulsion naturally corresponds to a decrease in eccentricities[9–11]. Note that in a first-order resonant chain, the actual period ratios between adjacent planets are not exactly equal to the resonant ratios (for example, 3:2)[12]. Instead, these ratios depend on the planets' eccentricities. The latter are all correlated to each other by a global resonant gauge, namely the total angular momentum of the system normalized by the reference resonant location (see Fig. 1a for, for example, a 3:2–3:2–3:2 four-planet chain and Methods). Thus, the period ratios and eccentricities do not evolve independently of each other. Processes such as dissipation that result in an increase of the normalized angular momentum (NAM) result in a predictable concurrent increase of all period ratios by lowering the eccentricities, which is associated with a rapid perihelion precession while maintaining formal libration of the resonant angles (known as resonant repulsion). It is striking that, whatever the initial NAM (that is, the eccentricities), after the dissipation-driven NAM increase, if the NAM is such that planets b

Table 1 | Chronological sequence of events leading to the assembly of the full TRAPPIST-1 chain in our model

Phase	Dynamical step	Main driving processes	Figure
0	Assembly of primordial b–c–d–e 3:2 chain; planets b–c–d fall into the inner cavity and planet e reaches the inner edge	Classical type-I migration with clearing of the inner disk and tidal dissipation	Extended Data Fig. 2
1	Planet e recedes with the inner edge and planets b–c–d divergently cross the 8:5–5:3 resonance through a NAM increase; OLT re-compactifies them	Expansion of the inner edge, tidal dissipation and outer Lindblad torque (OLT)	Fig. 1
2	The inner and outer subsystems join and the full TRAPPIST-1 chain is assembled	Tidal dissipation + OLT (inner system), classical type-I migration (outer system) and expansion of the inner edge	Fig. 2

https://doi.org/10.1038/s41550-024-02342-4

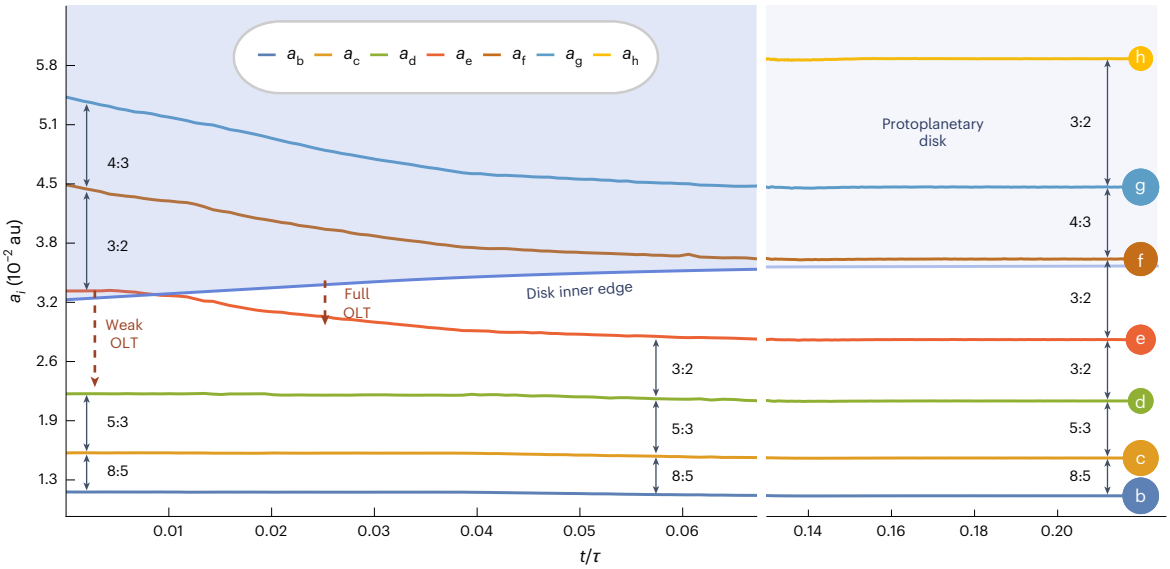

Fig. 2 | Joining of the inner and outer subsystems. Evolution of the semimajor axes shown with continuous coloured lines for all planets, which are also labelled by circles whose sizes reflect the observed size of each planet. In our favoured scenario, planet e followed the inner edge whereas planets b, c and d were in the inner cavity. Planets f, g and h joined the system later, undergoing inward disk-driven migration. The disk is depicted by the shaded area, with the lighter shading on the right indicating that the disk will eventually disperse. As planet g is more massive than f and h, it will probably capture f in resonance (the 4:3 being the favoured commensurability[5]) and the two planets will migrate in together. When f reaches the 3:2 resonance with e, the combined push from f and g is sufficient to dislodge planet e from the inner edge (shown as the blue line bordering the top shaded area). Driven by a full OLT, the orbit of planet e decays faster than those of f and g, and it approaches the 3:2 resonance with d. Planet h is the last one to migrate in. It captures g in the 3:2 resonance to complete the chain. au, astronomical unit.

and c are close to an 8:5 period ratio, then planets c and d are close to the 5:3 ratio. Thus, that planets b, c and d are observed to be close to these period ratios is no coincidence but evidence of a past evolution in the 3:2 resonant chain[7,8,13].

Figure 1 depicts this process quantitatively. Originating deep in a 3:2–3:2–3:2 resonant chain after migration and with a specific value of the NAM dictated by their eccentricities, planets b, c, d (in the disk cavity) and e evolve under dissipation, which increases their NAM. Figure 1b–d shows that all period ratios increase as expected[9,10,14]. When the period ratio T_c/T_b reaches 8:5, T_d/T_c simultaneously reaches 5:3. As these resonances are crossed divergently, the planets' eccentricities suddenly jump to larger values (Fig. 1c). If the eccentricities increase by more than a factor of two, as happens here given the measured planetary masses (note that planets b and c are the most massive in the inner system), theory predicts that the original first-order resonant chain is broken[14,15]. Thus, any further NAM increase no longer alters the T_c/T_b and T_d/T_c ratios (Fig. 1d). The planets are close to but not inside the 8:5 and 5:3 resonances because capture in these resonances is impossible during divergent migration. This scheme is a first step to a more accurate reconstruction of the dynamical history of the TRAPPIST-1 system, and it demonstrates that, although the presence of resonances indicates that migration must have occurred, other processes must have been at play concurrently with migration to shape its current architecture. If this scenario is appealing, the relevant questions are these: (1) What is the plausible origin of dissipation (NAM increase)? (2) How many planets were involved in the original resonant chain?

For the specific dissipation mechanism, a first possibility is efficient dissipation onto the planets (refs. 7,9–11,14; Methods). However, if such a dissipative force had been efficient enough to drive planets b, c and d into an 8:5–5:3 period ratio from a primordial 3:2–3:2 configuration, it would also have been able to rapidly dampen their eccentricities after their jump, thus restoring the 3:2–3:2 resonant chain and restarting the divergent evolution (Extended Data Fig. 1). Another possibility is that planets b and c were closer to the star than the inner edge of the disk because (1) they were pushed there by the migration of planets d and e, (2) they opened a gap in the disk, (3) the inner disk cavity expanded due to magnetic torque and photo-evaporation or (4) there was a combination of these processes. In this case, if planet d had remained at the inner disk's edge, planet c would have felt a negative one-sided Lindblad torque (OLT) from the disk (Methods), which would push c inwards, away from d. This is equivalent to a NAM increase due to the resonance gauge (Fig. 1a). However, because this push acts directly on planet c, it would have continued after the crossing of the 5:3 resonance between planets d and c, bringing the system away from the observed period ratio (unless a fortuitous and timely disappearance of the disk is invoked or a three-body resonance assembled between planets c, d and e at a suitable time, as in ref. 8).

Results

Building on these ideas, we propose here a way to obtain the repulsion of the orbits of TRAPPIST-1b, c and d that is largely insensitive to orbital damping parametrizations, pivoting instead on physical mechanisms that are expected to occur in the environment where the planets formed. We presuppose only that the inner edge of the disk receded with time[16,17] while the inner system was locked in the 3:2 resonant chain. We assume a four-planet 3:2 resonant chain like that simulated in Fig. 1, with planet e sitting at the inner edge of the disk being our preferred scenario (this is phase 0 in Table 1; Extended Data Fig. 2). As the disk's edge recedes, planet e recedes in concert, as it is anchored to it by the so-called co-orbital corotation torque[18]. Consequently, the separation between planets e and d increases in time, which causes the NAM and all period ratios to increase due to the resonance gauge. After the 8:5 and 5:3 resonance crossing and the breakdown of the 3:2 chain, planet e keeps receding, leaving planets b, c and d unaffected (Fig. 1d; in this simulation, the timescale τ, which describes the inner-edge recession rate, $\tau = r_{ed,0}/(dr_{ed}/dt)$, was 700 kyr, where $r_{ed}(t)$ is the radial location of the disk inner edge and $r_{ed,0}$ is its initial location). Simultaneously, planet d starts to migrate inward driven by an OLT. This migration is

https://doi.org/10.1038/s41550-024-02342-4

necessarily slow as only its outer 2:1 resonance falls in the disk[8]. Thus, planets c and d are now slowly convergently migrating on moderately eccentric orbits, which were pumped during the earlier divergent migration and resonance crossing, and they could be captured in the 5:3 resonance. Then, they keep slowly migrating inward together, with planet c capturing b in the 8:5 resonance. Eccentricity damping for planets inside the gas cavity is provided by tides inside the planets. The mysterious 8:5–5:3 resonance is thus established (phase 1 in Table 1).

In the current TRAPPIST-1 system, planet e is in the 3:2 period ratio with planet d, not arbitrarily away from it, as Fig. 1d would suggest. The most reasonable explanation is that planets f, g and h were not part of the original resonant chain but migrated into the inner part of the disk at some later time, as expected from the ringed-formation paradigm[17,19,20]. As planet f approached e, the two became captured in the 3:2 resonance, which excited planet e's eccentricity and dislodged it from the disk's inner edge[18,21]. In fact, planet g is more massive than f, so the f–g pair had probably already become locked into the most favoured[5] 4:3 resonance before approaching planet e, although this is not strictly necessary (Supplementary Information). Planet e thus left the inner edge and underwent OLT-driven inward migration approaching planet d. At this moment, no resonance with planet d had been re-established, so the inner system remained unaffected.

During its inward migration, planet e had a non-vanishing forced eccentricity due to the resonant interaction with f. Planet e must, however, have crossed a series of high-order resonances with planet d (9:5, 5:3 and 8:5), which it had to skip before reaching the 3:2 period ratio with d, where it is observed today. Capture in resonances of order higher than 1 is only a probabilistic event, whereas it is guaranteed for first-order resonances in the adiabatic limit. In addition, planet e experienced a NAM increase with respect to planet f due to the former's initially fast, full-OLT-driven migration (Methods). This evolution is naturally associated with the efficient damping of the eccentricities, which reduces the strength of the higher-order resonances and allows for a smooth joining of the inner and outer chains. The advantage of this mechanism is that it relies solely on the analytical evolution tracks depicted in Fig. 1 and not on enhanced disk-driven *e*-damping efficiencies (which may not be guaranteed[22,23], especially near the disk inner edge[24]). Our experiments show that, depending on the phases of the angles at approach and with different disk profiles, in up to 22% of simulations, the higher-order resonances between e and d are skipped and the 8:5–5:3 resonance for planets b–c–d is not disrupted, allowing for a successful joining of the inner and outer systems at the required period ratios at the end of this assembly phase (see 'Joining the inner and the outer systems' in the Supplementary Information, Extended Data Fig. 3 and Extended Data Table 1 for a parameter study with different surface densities). This presupposes that, to avoid planets c and d being subsequently captured in the 2:1 resonance, the inner edge has not moved outwards enough to make the period ratio between planets d and e larger than 2:1 before planet f approaches the inner system. A timing condition concerning the arrival of the outer planets to join the inner chain is implicit in a model that assumes a two-subsystem formation history. In our model, we also specifically require that planet f reaches the inner system before the inner edge has taken planets d and e outside the 2:1 period ratio (the timing of which is set by the average inner-edge recession rate after the 8:5–5:3 b–c–d resonance has been crossed). Finally, planet h, being less massive than g, migrates in and captures g into their 3:2 resonance at a later time, thus establishing the whole observed 8:5–5:3–3:2–3:2–4:3–3:2 chain (Fig. 2; see also phase 2 in Table 1).

After gas removal and the disappearance of the disk, the planets undergo a tidal evolution lasting several gigayears. Figure 3a shows that, for realistic tidal parameters[6], the eccentricities of all planets are consistent with those determined by observations[2], within the uncertainties, after about 2,500 to 3,000 circularization timescales of planet b. In the resonant chain that our model produces, the planets

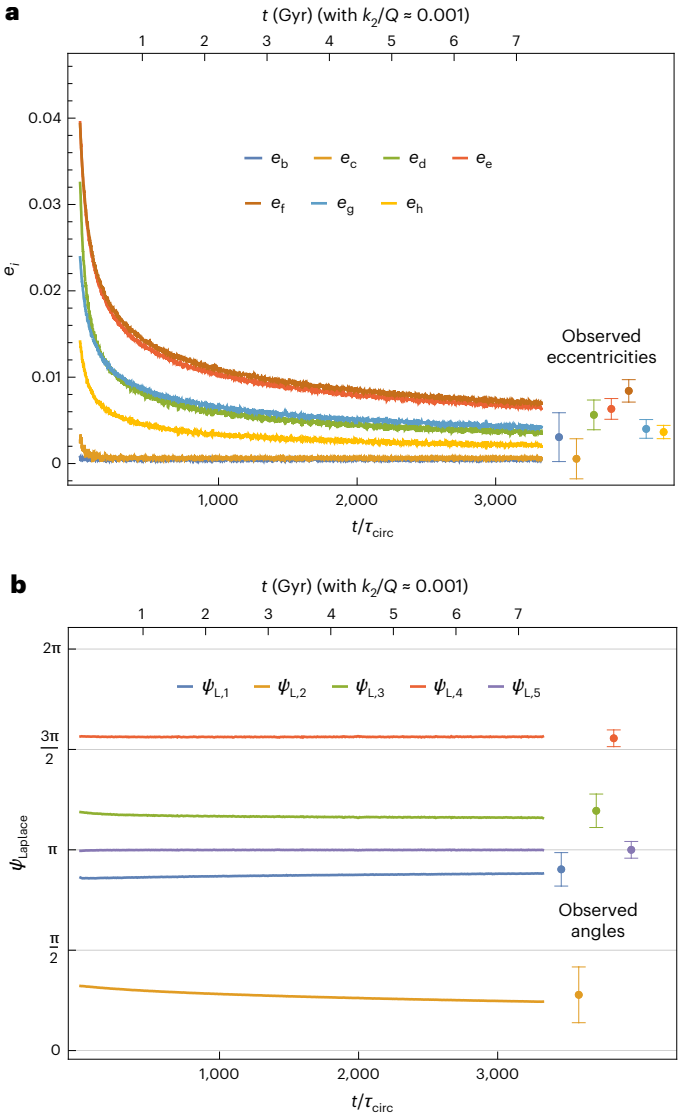

Fig. 3 | Post-nebular evolution under tidal dissipation of the TRAPPIST-1 system. a, Decay of the eccentricities due to tidal *e*-damping, showing that for reasonable tidal parameters, the presently observed eccentricities are reached after around 2,500 to 3,000 circularization timescales of planet b (error bars represent the 1σ confidence limits from ref. 2). **b**, Libration of the (reduced) Laplace angles defined in equation (3) compared with the libration centres and amplitudes (shown as error bars) observed from different draws from the posterior distribution from ref. 2.

are in Laplace resonances by triplets, as presently observed[2] (Fig. 3b). Moreover, neighbouring planet pairs between TRAPPIST-1c and g are in two-body mean motion resonances. The eccentricities of planets b and c reached vanishingly low values due to their tidal evolution (Fig. 3a), so that their 8:5 resonance angles stopped librating and presently show circulation. Still, all planets were in two-body resonances with their neighbours at the end of the disk-phase assembly of the system, which locked their period ratios close to the presently observed ones. This explains how the mysterious high-order 8:5–5:3 period ratios for planets b, c and d are not fortuitous but indicate a past evolution where both these resonances were active. Although the Laplace resonant states have been verified observationally[2], proving the two-body resonance states requires precise knowledge of the longitudes of the orbital pericentres, which is difficult to achieve. Improved characterization of the dynamical state of the TRAPPIST-1 system will eventually allow us to verify our model prediction.

Discussion

Our model builds on previous ideas such as the separation into two subsystems[7,8] and the role of the disk inner edge in anchoring planets[17,25]. Here, we are able to explain the complex orbital architecture of the TRAPPIST-1 planets in a model that is largely insensitive to specific migration and eccentricity-damping efficiency parameters by pivoting on physical processes that are expected to occur in protoplanetary disks. The recession of the inner edge provides a natural dynamical pathway to assemble the otherwise unlikely[5] 8:5–5:3 resonances. Such an inner-edge evolution has been predicted by theoretical models[16] but is presently inaccessible to observations. Our work provides indirect evidence of its role in the assembly of the TRAPPIST-1 system. In our model, the (unknown) rate of the inner-edge recession rate after the 8:5–5:3 b–c–d resonance crossing should not be so fast that planets d–e exceed the 2:1 period ratio before the arrival time (also unknown) of planet f ('Planets' formation history and physical characterisation' in the Supplementary Information). However, note that the location of the inner edge is set by the magnetic truncation radius $R_t \propto \dot{M}_g^{-2/7}$ (ref. 16), with the gas accretion rate $\dot{M}_g \propto (1 + t/\tau_{acc})^{-\eta}$, where τ_{acc} is a (time-averaged) accretion timescale[26] and $\eta \gtrsim 1$, as expected for viscous accretion[27]. Thus, the inner-edge recession rate is expected to slow down over time. Moreover, our model shows that the strong eccentricity damping needed to obtain these specific configurations can be the result of divergent migration in a resonant configuration inside the disk cavity, rather than direct damping from the disk, thus removing a tension with the hydrodynamical simulations[8]. All these ingredients, which are essential for reproducing the TRAPPIST-1 system within our current understanding of planet–disk interactions, may have played an important role in other planetary systems as well and open the possibility of a precise reconstruction of their dynamical history, as we have done here for the TRAPPIST-1 system.

Methods

Mean motion resonances and Laplace angles

The analytical treatment of chains of mean motion resonances is the subject of many works[12,28,29] and is reasonably well understood, so we do not reproduce it here. We detail only the main points used in the analytical calculations.

Consider N planets labelled by their distance from the star. If planets i and $i+1$ are close to a $p_i + q_i{:}p_i$ mean motion resonance, with p_i and q_i integers, then the period ratio $T_{i+1}/T_i \simeq (p_i + q_i)/p_i$. After expanding the gravitational potential describing planet–planet interactions in a Fourier series, all terms of the potential that do not contain the resonant combination $(p_i + q_i)\lambda_{i+1} - p_i\lambda_i$ can be averaged out (dropped), as they are fast angles. Moreover, by the d'Alembert rules, the only harmonics that appear at lowest order in the eccentricities are

$$\begin{aligned}
\psi_i^{(q_i,0)} &:= (p_i + q_i)\lambda_{i+1} - p_i\lambda_i - q_i\varpi_i \\
&\quad \left(\text{associated with a term proportional to } e_i^{q_i}\right), \\
\psi_i^{(q_i-1,1)} &:= (p_i + q_i)\lambda_{i+1} - p_i\lambda_i - (q_i - 1)\varpi_i - \varpi_{i+1} \\
&\quad \left(\text{term proportional to } e_i^{q_i-1}e_{i+1}^{1}\right), \\
\psi_i^{(q_i-2,2)} &:= (p_i + q_i)\lambda_{i+1} - p_i\lambda_i - (q_i - 2)\varpi_i - 2\varpi_{i+1} \\
&\quad \left(\text{term proportional to } e_i^{q_i-2}e_{i+1}^{2}\right), \\
&\ldots, \\
\psi_i^{(0,q_i)} &:= (p_i + q_i)\lambda_{i+1} - p_i\lambda_i - q_i\varpi_{i+1}\left(\text{term proportional to } e_{i+1}^{q_i}\right).
\end{aligned} \tag{1}$$

Here, λ_i and ϖ_i are the planets' mean longitudes and longitudes of pericentres, respectively. The ψ_i are the (two-body) resonant angles for the $p_i + q_i{:}p_i$ mean motion resonance and represent the relevant interaction terms that drive the dynamics. For example, for the 3:2 mean motion resonance between planets TRAPPIST-d and e, $p = 2$ and $q = 1$ (first-order resonance) and there are two resonant angles: $3\lambda_e - 2\lambda_d - \varpi_d$ and $3\lambda_e - 2\lambda_d - \varpi_e$. For the 5:3 mean motion resonance between planets TRAPPIST-c and d, $p = 3$ and $q = 2$ (second-order resonance), and there are three resonant angles: $5\lambda_d - 3\lambda_c - 2\varpi_c$, $5\lambda_d - 3\lambda_c - \varpi_c - \varpi_d$ and $5\lambda_d - 3\lambda_c - 2\varpi_d$. When two planets are in resonance, some or all resonant angles are librating, which represents a dynamical state contained within a resonant island in phase space. Note that all resonant interaction terms are proportional to the eccentricities to the power q_i, and they, therefore, contribute less for larger q_i or smaller eccentricities (the resonant islands cover less volume in phase space).

Note that if a triplet of consecutive planets i, $i+1$ and $i+2$ lies in a resonant chain, one can build appropriate combinations of the two-body resonant angles of the two pairs to obtain an angle that depends on the mean longitudes of the three planets but not on any of the pericentres. For example, with a $p_i + 1{:}p_i$ resonance for the inner pair and $p_{i+1} + 1{:}p_{i+1}$ for the outer pair, then the combination of the resonant angles $(p_i + 1)\lambda_{i+1} - p_i\lambda_i - \varpi_{i+1}$ (inner pair's resonance and pericentre of the outer planet) and $(p_{i+1} + 1)\lambda_{i+2} - p_{i+1}\lambda_{i+1} - \varpi_{i+1}$ (outer pair's resonance and pericentre of the inner planet) removes the dependence on the pericentre ϖ_{i+1}:

$$\begin{aligned}
\psi_i^{(p_{i+1}+1,-(p_{i+1}+p_i+1),p_i)} &:= ((p_{i+1} + 1)\lambda_{i+2} - p_{i+1}\lambda_{i+1} - \varpi_{i+1}) \\
&\quad - ((p_i + 1)\lambda_{i+1} - p_i\lambda_i - \varpi_{i+1}) \\
&= (p_{i+1} + 1)\lambda_{i+2} - (p_{i+1} + p_i + 1)\lambda_{i+1} + p_i\lambda_i.
\end{aligned} \tag{2}$$

Such three-body angles are called Laplace angles. If both resonant angles are librating, the Laplace angle must also librate. As the Laplace angles for triplets of planets do not involve the pericentres but only the mean longitudes λ_i, which are determined precisely by the transit times, their libration is easier to observe compared to the libration of the two-body resonance angles in exoplanetary systems, for which information about the pericentres is harder to obtain.

The Laplace angles that have been reported by ref. 2 to be librating in the TRAPPIST-1 chain are

$$\begin{aligned}
\psi_{L,1} &= 2\lambda_b - 5\lambda_c + 3\lambda_d = -(3\lambda_c - 2\lambda_b - \varpi_c) + (3\lambda_d - 2\lambda_c - \varpi_c), \\
\psi_{L,2} &= 1\lambda_c - 3\lambda_d + 2\lambda_e = [-(5\lambda_d - 3\lambda_c - 2\varpi_d) + 2(3\lambda_e - 2\lambda_d - \varpi_d)]/3, \\
\psi_{L,3} &= 2\lambda_d - 5\lambda_e + 3\lambda_f = -(3\lambda_e - 2\lambda_d - \varpi_e) + (3\lambda_f - 2\lambda_e - \varpi_e), \\
\psi_{L,4} &= 1\lambda_e - 3\lambda_f + 2\lambda_g = [-(3\lambda_f - 2\lambda_e - \varpi_f) + (4\lambda_g - 3\lambda_f - \varpi_f)]/2, \\
\psi_{L,5} &= 1\lambda_f - 2\lambda_g + 1\lambda_h = [-(4\lambda_g - 3\lambda_f - 2\varpi_g) + (3\lambda_h - 2\lambda_g - \varpi_g)]/3.
\end{aligned} \tag{3}$$

Note that some of these angles are obtained from two-body resonant angles after dividing by an integer (the greatest common divisor of the integers multiplying the angles)[30]. However, only non-reduced angles actually appear in the Fourier expansion of the gravitational potential. Division by an integer is equivalent to a phase-folding of the angles.

Resonant equilibria for a 3:2 resonance chain

If all planet pairs in a planetary system are in $p_i + 1{:}p_1$ two-body resonances, planet–planet interaction terms that do not involve resonant angles can be dropped. Thus, the resonant model will not depend on any one of the longitudes λ_i but only on their resonant combinations. This introduces, in a regime without external dissipation or forcing, an extra constant of motion $\mathcal{K}$, a resonant scaling parameter[12,31]. For an N-planet 3:2 chain, this constant of motion takes the form[11]

$$\mathcal{K} = \sum_{i=1}^{N}\left(\frac{2}{3}\right)^{i-1} m_i\sqrt{\mu_0 a_i}, \tag{4}$$

where m_i are the planets' masses and $\mu_0 = \mathcal{G}M_*$ is the standard gravitational parameter of the central star. We define the NAM as $\mathcal{L}/\mathcal{K}$, where $\mathcal{L} = \sum_{i=1}^{N} m_i\sqrt{\mu_0 a_i(1 - e_i^2)}$ is the total (orbital) angular momentum, which

is a conserved quantity in a non-dissipative regime. As the planetary problem is scale-free and $\mathcal{K}$ is proportional to $a^{1/2}$, this is equivalent to reasoning in terms of semimajor axis ratios rather than the absolute semimajor axes. The global state of the resonant system in rescaled quantities is, thus, completely determined by the NAM.

With this scheme at hand, using the analytical treatment of resonances (for example, ref. 11), one can find, for a given value of the NAM, a resonant equilibrium in phase space by imposing libration of the resonant angles. This results in curves parametrized by the NAM that track the resonant states as a function of the orbital elements, as shown in Fig. 1. That the resonant locations do not coincide with period ratios exactly equal to the nominal ratios $(p_i+1)/p_i$ but deviate away from exact commensurability for small eccentricities is simple to understand. At the centre of the resonant island, the libration of a resonant angle like $(p_i+1)\lambda_{i+1}-p_i\lambda_i-\varpi$ (where ϖ is either ϖ_i or ϖ_{i+1}) imposes that $(p_i+1)\Omega_{\mathrm{Kep},i+1}-p_i\Omega_{\mathrm{Kep},i}=\frac{\mathrm{d}}{\mathrm{d}t}\left[(p_i+1)\lambda_{i+1}-p_i\lambda_i\right]=\frac{\mathrm{d}\varpi}{\mathrm{d}t}=:\dot{\varpi}$. As $\dot{\varpi}$ is proportional to $1/e$, for faster perihelion precession rates (lower eccentricities), the orbital periods of the planets will be farther away from exact commensurability. The dotted-dashed orange line in Fig. 1b is the same curve but in the period ratio space T_c/T_b versus T_d/T_c, showing how, by starting very close to a 3:2–3:2 period ratio commensurability, one naturally crosses the 8:5–5:3 chain for a system undergoing a NAM increase. This peculiarity of the phase space near a 3:2–3:2 chain has already been observed by, for example, ref. 13.

Planet–disk interactions, disk structure and modelling of the inner edge

To model planet–disk interactions, we follow the prescription of ref. 32 derived from three-dimensional hydrodynamical simulations for planets with planet-to-star mass ratios like those of the TRAPPIST-1 system. This prescribes the torque and eccentricity damping felt by a planet deeply embedded in the disk[33] in a similar way to other works on the TRAPPIST-1 system[5,6,8]:

$$\Gamma_{\mathrm{tl}}=\left(\frac{\mathrm{d}\mathcal{L}}{\mathrm{d}t}\right)_{\mathrm{tl}}=-\frac{\mathcal{L}}{\tau_{\mathrm{mig,tl}}},\qquad \left(\frac{\mathrm{d}e}{\mathrm{d}t}\right)_{\mathrm{tl}}=-\frac{e}{\tau_{e,\mathrm{tl}}}. \tag{5}$$

As in refs. 5,6, we use the migration prescription from ref. 32, which is consistent with three-dimensional hydrodynamical simulations of planets of this mass range embedded in disks. We discuss in 'Calculation of one-sided Lindblad torques' in the Supplementary Information the modelling of the OLT felt by a planet that has fallen into the cavity.

We model the static disk surface density as a power law multiplied by a factor to reproduce the drop in gas density at the inner cavity:

$$\Sigma(r)=\mathcal{R}\Sigma_0\left(\frac{r}{r_0}\right)^{-\alpha_{\Sigma,0}}, \tag{6}$$

where Σ_0 is a reference density at a reference radius r_0 (we take, for example, $r_0=0.025$ au, which is between the current locations of planets d and e) and $\alpha_{\Sigma,0}$ is the slope of the unbroken-power-law disk (at larger separations away from the inner edge). We chose an underlying power-law exponent $\alpha_{\Sigma,0}=3/5$, which is appropriate for the viscously heated region of the disk, as was done in ref. 6. For the surface density Σ_0, we tested values spanning different orders of magnitude (Extended Data Table 1). We used a factor $\mathcal{R}$ given by

$$\mathcal{R}=\mathcal{R}(r;r_{\mathrm{ed}},h_{\mathrm{ed}},w_{\mathrm{ed}})=G\left(\frac{r-r_{\mathrm{ed}}}{h_{\mathrm{ed}}r_{\mathrm{ed}}w_{\mathrm{ed}}}\right), \tag{7}$$

where r_{ed} is the reference location of the inner edge, $h_{\mathrm{ed}}:=h(r_{\mathrm{ed}})$ is the aspect ratio of the disk at r_{ed} and w_{ed} represents an inner-edge width, which we take to be 1, although we also experimented with a value of 0.5. We consider a constant aspect ratio across the disk for simplicity, $h(r)=h_0$, and thus the flaring index $\beta_{\mathrm{fl}}=0$, as in previous works[6,8]. We chose $h_0=0.05$, but the actual value of the aspect ratio has the sole effect of rescaling the capture eccentricities attained after the establishment of the 3:2 chain, as $e_{\mathrm{capt}}\propto h$. However, after the resonant repulsion driven by the receding inner edge, this information is completely lost. In this work, the function G is given by

$$G(\xi):=\frac{\tanh(2\xi)+1}{2}, \tag{8}$$

which satisfies $G(\xi)\approx 0$ if $\xi\lesssim -1$ and $G(\xi)\approx 1$ if $\xi\gtrsim 1$. The choice of the hyperbolic tangent was informed by non-ideal magneto-hydrodynamical simulations[34] and has been used in many N-body works[35,36]. The specific functional form differs, however, slightly from similar descriptions of disk inner edges in previous papers[35,36], as it has the advantage of being differentiable at all radii. This means that the local surface density slope

$$\alpha_\Sigma=\alpha_\Sigma(r):=-\frac{\mathrm{d}\log\Sigma}{\mathrm{d}\log r}(r) \tag{9}$$

is a continuous function such that $\alpha_\Sigma(r)\approx\alpha_{\Sigma,0}$ for $r\gtrsim r_{\mathrm{ed}}$. The continuity of the local slope $\alpha_\Sigma(r)$ is an advantage with respect to previous prescriptions when calculating the torque felt by a planet at the inner edge, which depends on α_Σ, as it eliminates the presence of unphysical discontinuities in the torque.

Once the inner b–c–d–e 3:2–3:2–3:2 chain is built, we assumed that planets b, c and d fall into the inner cavity, whereas planet e remains in the disk and reaches the inner disk edge. We mimic this in our N-body simulations as an evolution in which the gas around planets b, c and d is slowly removed (a clearing of the inner region of the disk). To this effect, we implemented a time-dependent gas surface density prescription given by

$$\Sigma(r,t)=\tilde{\mathcal{R}}(t)\Sigma_0\left(\frac{r}{r_0}\right)^{-\alpha_{\Sigma,0}}. \tag{10}$$

The new time-dependent $\tilde{\mathcal{R}}$ is taken here as

$$\tilde{\mathcal{R}}(t):=\mathcal{R}_{\mathrm{in}}+(\mathcal{R}_{\mathrm{fin}}-\mathcal{R}_{\mathrm{in}})\tilde{G}\left(\frac{t-t_0}{t_{\mathrm{in}}-t_0}\right), \tag{11}$$

where $\mathcal{R}_{\mathrm{in}}=\mathcal{R}(r;r_{\mathrm{ed,in}},h_{\mathrm{ed,in}},w_{\mathrm{ed,in}})$, $\mathcal{R}_{\mathrm{fin}}=\mathcal{R}(r;r_{\mathrm{ed,fin}},h_{\mathrm{ed,fin}},w_{\mathrm{ed,fin}})$ and $\tilde{G}(\xi)$ is a function that is zero for $\xi<0$, 1 for $\xi>1$ and smooth for $0<\xi<1$. We take, for example,

$$\tilde{G}(\xi):=\begin{cases}0, & \text{if } \xi\le 0,\\ (\cos(\pi(\xi+1))+1)/2, & \text{if } 0<\xi<1,\\ 1, & \text{if } \xi\ge 1.\end{cases} \tag{12}$$

The effect of equations (10) through (12) is to simulate the clearing of the inner region of the disk so that the final inner-edge position is at $r_{\mathrm{ed,fin}}$, which we assumed lies between the orbits of planets d and e. The exact functional form is unimportant, as is the timescale over which this evolution takes place $(t_{\mathrm{in}}-t_0)$, as long as the evolution is adiabatic ('Evolution of the Trappist-1b,c,d,e inner system: capture in the 3:2 chain and clearing of the inner disk' in the Supplementary Information).

The shift in the inner-edge position is simply accomplished by changing the value of r_{ed} in equation (7). We experimented with various functional forms for the drift of the inner edge. All gave similar results based on the theoretical tracks depicted in Fig. 1. At the end of the assembly of the TRAPPIST-1 system, the disk is removed by multiplying the surface density by an exponentially decreasing function of time.

Tidal dissipation

As the TRAPPIST-1 planets are very close to the central star, they are expected to experience substantial tidal dissipation[10,37]. In our simulations, tidal effects act as eccentricity-damping dissipative forces with

$$\left(\frac{\mathrm{d}e}{\mathrm{d}t}\right)_{\mathrm{tide}} = -e\frac{21\Omega_{\mathrm{Kep}}}{2}\frac{k_2}{Q}\frac{M_*}{m_{\mathrm{pl}}}\left(\frac{R}{a}\right)^5 =: -\frac{e}{\tau_{e,\mathrm{tide}}}, \quad (13)$$

where R is the planet's radius, Q is the tidal quality factor and k_2 is the planetary Love number[37]. Tides inside the star are neglected. There are large uncertainties on the value of k_2/Q, but this can be estimated to be of the order of 10^{-3} from dynamical arguments[7,8] or interior modelling[6]. Note that the role of eccentricity damping in the assembly phase is to counteract the push provided by the torque[29] (in this case the outer Lindblad torque). As the torque is proportional to the local surface density around the inner edge of the disk, any uncertainty in the value of k_2/Q can be carried over to a modified local surface density.

Data availability

The time series of the simulations displayed in the manuscript and the data used to plot the analytical curves in Fig. 1 are available at https://github.com/GabrielePichierri/FormingTrappist-1. Data corresponding to the observed physical and orbital state of the TRAPPIST-1 system were taken from https://github.com/ericagol/TRAPPIST1_Spitzer.

Code availability

The *N*-body integrations were run using the publicly available SWIFT subroutine package (https://www.boulder.swri.edu/~hal/swift.html), which has been modified with the extra forces needed. The other subroutines are available upon request from the corresponding author (G.P.). The analytical calculations were performed using the computational software Mathematica.

References

1. Luger, R. et al. A seven-planet resonant chain in TRAPPIST-1. *Nat. Astron.* **1**, 0129 (2017).
2. Agol, E. et al. Refining the transit-timing and photometric analysis of TRAPPIST-1: masses, radii, densities, dynamics, and ephemerides. *Planet. Sci. J.* **2**, 1 (2021).
3. Kley, W. & Nelson, R. P. Planet-disk interaction and orbital evolution. *Annu. Rev. Astron. Astrophys.* **50**, 211–249 (2012).
4. Tamayo, D., Rein, H., Petrovich, C. & Murray, N. Convergent migration renders TRAPPIST-1 long-lived. *Astrophys. J. Lett.* **840**, L19 (2017).
5. Teyssandier, J., Libert, A.-S. & Agol, E. TRAPPIST-1: dynamical analysis of the transit-timing variations and origin of the resonant chain. *Astron. Astrophys.* **658**, A170 (2022).
6. Brasser, R., Pichierri, G., Dobos, V. & Barr, A. C. Long-term tidal evolution of the TRAPPIST-1 system. *Mon. Not. R. Astron. Soc.* **515**, 2373–2385 (2022).
7. Papaloizou, J. C. B., Szuszkiewicz, E. & Terquem, C. The TRAPPIST-1 system: orbital evolution, tidal dissipation, formation and habitability. *Mon. Not. R. Astron. Soc.* **476**, 5032–5056 (2018).
8. Huang, S. & Ormel, C. W. The dynamics of the TRAPPIST-1 system in the context of its formation. *Mon. Not. R. Astron. Soc.* **511**, 3814–3831 (2022).
9. Lithwick, Y. & Wu, Y. Resonant repulsion of Kepler planet pairs. *Astrophys. J. Lett.* **756**, L11 (2012).
10. Batygin, K. & Morbidelli, A. Dissipative divergence of resonant orbits. *Astron. J.* **145**, 1 (2013).
11. Pichierri, G., Batygin, K. & Morbidelli, A. The role of dissipative evolution for three-planet, near-resonant extrasolar systems. *Astron. Astrophys.* **625**, A7 (2019).
12. Batygin, K. & Morbidelli, A. Analytical treatment of planetary resonances. *Astron. Astrophys.* **556**, A28 (2013).
13. Charalambous, C., Martí, J. G., Beaugé, C. & Ramos, X. S. Resonance capture and dynamics of three-planet systems. *Mon. Not. R. Astron. Soc.* **477**, 1414–1425 (2018).
14. Delisle, J.-B., Laskar, J. & Correia, A. C. M. Resonance breaking due to dissipation in planar planetary systems. *Astron. Astrophys.* **566**, A137 (2014).
15. Pichierri, G. & Morbidelli, A. The onset of instability in resonant chains. *Mon. Not. R. Astron. Soc.* **494**, 4950–4968 (2020).
16. Liu, B., Ormel, C. W. & Lin, D. N. C. Dynamical rearrangement of super-Earths during disk dispersal. I. Outline of the magnetospheric rebound model. *Astron. Astrophys.* **601**, A15 (2017).
17. Ormel, C. W., Liu, B. & Schoonenberg, D. Formation of TRAPPIST-1 and other compact systems. *Astron. Astrophys.* **604**, A1 (2017).
18. Masset, F. S. Planet disk interactions. *EAS Publ. Ser.* **29**, 165–244 (2008).
19. Schoonenberg, D., Liu, B., Ormel, C. W. & Dorn, C. Pebble-driven planet formation for TRAPPIST-1 and other compact systems. *Astron. Astrophys.* **627**, A149 (2019).
20. Morbidelli, A. et al. Contemporary formation of early Solar System planetesimals at two distinct radial locations. *Nat. Astron.* **6**, 72–79 (2022).
21. Fendyke, S. M. & Nelson, R. P. On the corotation torque for low-mass eccentric planets. *Mon. Not. R. Astron. Soc.* **437**, 96–107 (2014).
22. Pichierri, G., Bitsch, B. & Lega, E. A recipe for orbital eccentricity damping in the type-I regime for low-viscosity 2D discs. *Astron. Astrophys.* **670**, A148 (2023).
23. Pichierri, G., Bitsch, B. & Lega, E. A recipe for eccentricity and inclination damping for partial-gap opening planets in 3D disks. *Astrophys. J.* **967**, 111 (2024).
24. Ataiee, S. & Kley, W. Pushing planets into an inner cavity by a resonant chain. *Astron. Astrophys.* **648**, A69 (2021).
25. Masset, F. S., Morbidelli, A., Crida, A. & Ferreira, J. Disk surface density transitions as protoplanet traps. *Astrophys. J.* **642**, 478–487 (2006).
26. Batygin, K. & Adams, F. C. Magnetic and gravitational disk-star interactions: an interdependence of PMS stellar rotation rates and spin-orbit misalignments. *Astrophys. J.* **778**, 169 (2013).
27. Manara, C. F. et al. Demographics of young stars and their protoplanetary disks: lessons learned on disk evolution and its connection to planet formation. In *Proc. Protostars and Planets VII* (eds Inutsuka, S. et al.) 539–565 (NSF, 2023).
28. Delisle, J.-B. Analytical model of multi-planetary resonant chains and constraints on migration scenarios. *Astron. Astrophys.* **605**, A96 (2017).
29. Pichierri, G., Morbidelli, A. & Crida, A. Capture into first-order resonances and long-term stability of pairs of equal-mass planets. *Celest. Mech. Dyn. Astron.* **130**, 54 (2018).
30. Siegel, J. C. & Fabrycky, D. Resonant chains of exoplanets: libration centers for three-body angles. *Astron. J.* **161**, 290 (2021).
31. Michtchenko, T. A., Beaugé, C. & Ferraz-Mello, S. Dynamic portrait of the planetary 2/1 mean-motion resonance. I. Systems with a more massive outer planet. *Mon. Not. R. Astron. Soc.* **387**, 747–758 (2008).
32. Cresswell, P. & Nelson, R. P. Three-dimensional simulations of multiple protoplanets embedded in a protostellar disc. *Astron. Astrophys.* **482**, 677–690 (2008).
33. Tanaka, H., Takeuchi, T. & Ward, W. R. Three-dimensional interaction between a planet and an isothermal gaseous disk. I. Corotation and Lindblad torques and planet migration. *Astrophys. J.* **565**, 1257–1274 (2002).
34. Flock, M., Fromang, S., Turner, N. J. & Benisty, M. 3D radiation nonideal magnetohydrodynamical simulations of the inner rim in protoplanetary disks. *Astrophys. J.* **835**, 230 (2017).

35. Izidoro, A. et al. Breaking the chains: hot super-Earth systems from migration and disruption of compact resonant chains. *Mon. Not. R. Astron. Soc.* **470**, 1750–1770 (2017).
36. Izidoro, A. et al. Formation of planetary systems by pebble accretion and migration. Hot super-Earth systems from breaking compact resonant chains. *Astron. Astrophys.* **650**, A152 (2021).
37. Goldreich, P. & Soter, S. Q in the Solar System. *Icarus* **5**, 375–389 (1966).

Acknowledgements

G.P. is grateful for support from the European Research Council (Starting Grant No. 757448-PAMDORA) and from the Barr Foundation for their financial support. A.M. is grateful for support from the European Research Council (Advanced Grant No. HolyEarth 101019380) and to Caltech for the visiting professor programme, which he could benefit from. K.B. is grateful to Caltech's Center for Comparative Planetology, the David and Lucile Packard Foundation and the National Science Foundation (Grant No. AST 2109276) for their generous support. This study is supported by the Research Council of Norway through its Centres of Excellence funding scheme (Project No. 332523 PHAB to R.B.). G.P. thanks M. Goldberg and B. Bitsch for helpful discussions.

Author contributions

G.P. conceived the model, designed the *N*-body simulations, modified the *N*-body code with extra routines to model more effects (migration, the inner edge of the disk and its evolution, and the OLT implementation), performed the numerical experiments, analysed the data, produced the figures and wrote the paper. A.M. conceived of and designed the model, suggested using resonant repulsion as a mechanism for circularizing the orbits at the inner edge, supplied part of the code for the model migration and wrote the paper. K.B. contributed the part of the *N*-body code that models the planetary tides and helped in designing the *N*-body simulations and in writing the paper. R.B. originated the discussion on the formation of the TRAPPIST-1 system, contributed data on the planets' physical and orbital properties and helped in writing the paper.

Competing interests

The authors declare no competing interests.

Additional information

Extended data is available for this paper at https://doi.org/10.1038/s41550-024-02342-4.

Supplementary information The online version contains supplementary material available at https://doi.org/10.1038/s41550-024-02342-4.

Correspondence and requests for materials should be addressed to Gabriele Pichierri.

Peer review information *Nature Astronomy* thanks the anonymous reviewers for their contribution to the peer review of this work.

https://doi.org/10.1038/s41550-024-02342-4

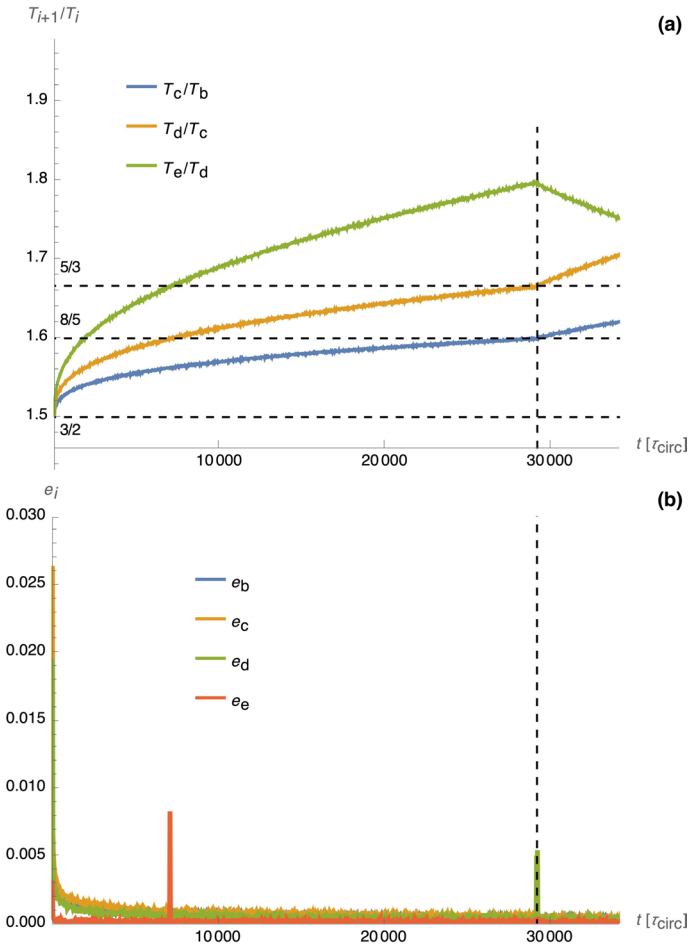

Extended Data Fig. 1 | Purely tidal evolution of a Trappist-1b,c,d,e 3:2 – 3:2 – 3:2 chain. This evolution is similar to the one in Fig. 1, with the sole difference that NAM increase is instead provided by a dissipative force onto the planets inside the cavity. The evolution of period ratios (panel (a)) and eccentricities (panel (b)) is equivalent to that of Fig. 1 as expected, until the crossing of the double 8:5 – 5:3 resonance. At this point, unlike the case of NAM increase provided by a receding inner edge (Fig. 1), the dissipative force quickly re-establishes a 3:2 – 3:2 commensurability between planets b,c and d by efficiently lowering their eccentricities, thus restoring the resonant repulsion mechanism. Thus, T_c/T_b and T_d/T_c continue to grow past the observed 8:5 – 5:3 ratios, while planet e jumps out of resonance. This shows that direct dissipation onto the planets alone is not as robust a mechanism to explain the assembly of the inner-most 8:5 – 5:3 chain.

https://doi.org/10.1038/s41550-024-02342-4

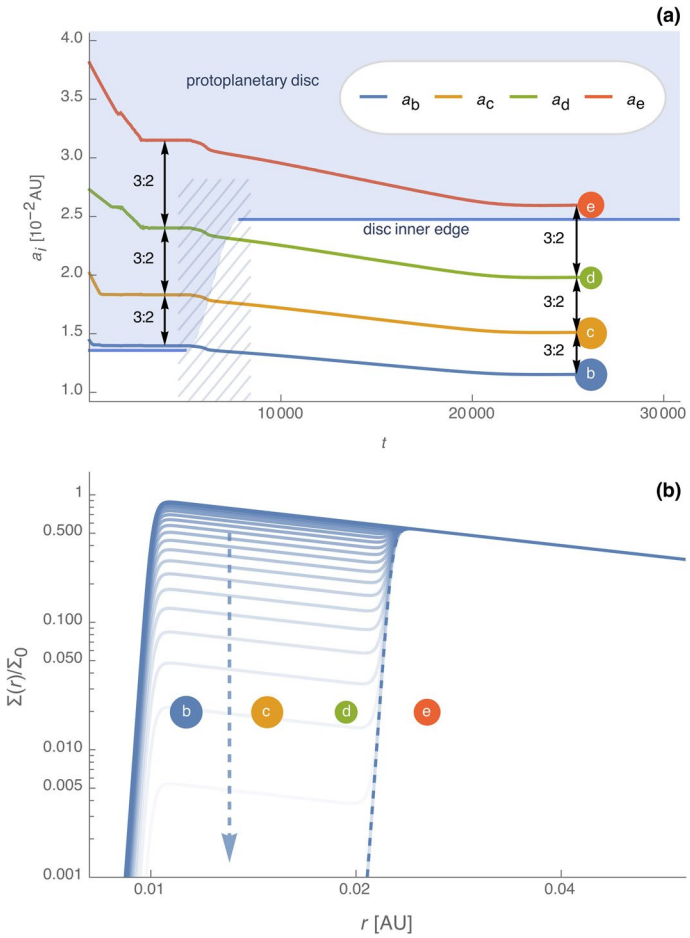

Extended Data Fig. 2 | Assembly of a primordial 3:2 chain among planets Trappist-1b,c,d,e. Planets b,c,d,e form a 3:2 – 3:2 – 3:2 chain inside the disc (top shade area), followed by planets b, c and d entering the inner disc cavity, with planet e migrating and reaching the inner edge (the blue line enclosing the top shaded area). The evolution of the semi-major axes is plotted in panel (a). Each planet is indicated by a coloured circle whose size reflects the observed size of the planet. This N-body simulation mimics the entry of planets b, c and d inside the inner cavity as a removal of the inner portion of the disc surrounding these planets. The corresponding evolution of the surface density in this phase is sketched in the panel (b), where the arrow indicates the drop of surface density in time (see also the dashed region in panel (a) and the shift in the initial and final position of the inner edge).

https://doi.org/10.1038/s41550-024-02342-4

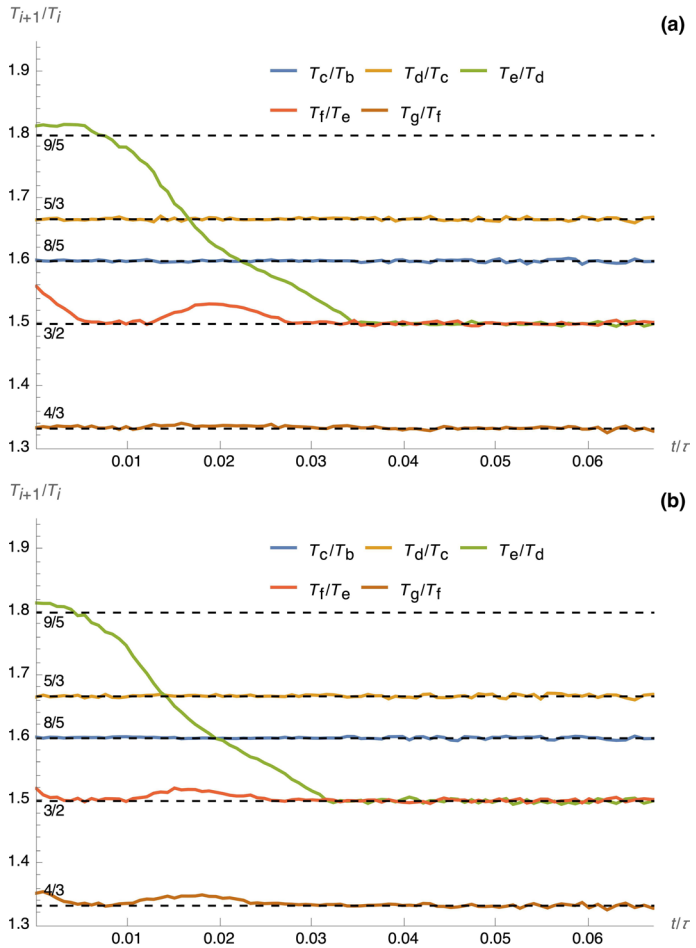

Extended Data Fig. 3 | The planets' period ratios while the inner and outer subsystems are joined. Two examples of the joining of the inner system (with b, c and d in their 8:5 – 5:3 resonance) with the outer system are shown (see also the left panel of Fig. 2). Panel (a): planets f and g already in their 4:3 resonance. Panel (b): planets f and g close, but not yet inside, their 4:3 resonance. The evolution in both cases is very similar: planet e interacts with planet f via their 3:2 resonance (red curve) and starts to migrate inward with respect to planet d (green curve). Note in particular that, when planet e crosses high-order resonances with planet d, the period ratio T_f/T_e increases slightly, which is associated with very efficient e_e-damping (see Fig. 1a on the structure of 3:2 resonances). This efficient damping helps in preventing spurious captures in unwanted high-order resonances.

https://doi.org/10.1038/s41550-024-02342-4

Extended Data Table 1 | Statistical study of the successful joining of the inner and outer system

Σ_0 [g/cm^2]	Success Probability	
	8:5 – 5:3 assembled	8:5 – 5:3 not assembled
5×10^1	0%	0%
2.5×10^2	14%	22%
5×10^2	22%	20%
2.5×10^3	16%	4%
5×10^3	22%	2%

We detail the success probabilities of joining the Trappist-1b,c,d Trappist-1,e,f,g subsystems for different surface densities Σ_0 (cfr. Eq. (6), with r_0=0.025 AU, $\alpha_{\Sigma,0}$=3/5). The left and right columns represent the extreme cases where the inner 8:5 – 5:3 resonance between planets b, c, and d has already been established by the OLT on planet d or not, respectively.